

## Investigation of Velocity Distribution and Turbulent Energy for the Different Tip Shaped Projectiles

Mehmet Hanifi DOĞRU\*<sup>1</sup>

<sup>1</sup>Gaziantep Üniversitesi, Aeronautics and Aerospace Faculty, Pilotage Department, Gaziantep

Geliş tarihi: 15.03.2017

Kabul tarihi: 25.09.2017

### Abstract

Velocity distribution on the projectile is a critical specification in terms of the range and perforation concept of the projectile. The shape of the projectile affects the amount of perforation energy. In this study, velocity distribution and turbulence energy are investigated for the projectiles on different tip shapes by using Solidworks Flow Simulation. Three different projectile nose shapes are examined in this study (sharpen, semi-rounded and rounded). Initial velocity is accepted to be 500 m/s for all situations. It is determined that the velocity is less affected on the sharpen type projectile where the penetration becomes easier. At the end of this study, velocity and pressure distribution on the penetrators in different tip geometries are obtained. The maximum velocity decrease at the tip of penetrator is found to be as 57.5% for the rounded type projectile. When the results are investigated, it is clear that velocity loss is about 22.2% in sharp type projectile.

**Keywords:** Velocity distribution, Turbulent energy, Projectile, Flow simulation, Tip geometry

### Farklı Uç Şeklindeki Mermiler için Hız Dağılımı ve Türbülans Enerjisinin Araştırılması

#### Öz

Mermi üzerindeki hız dağılımı, merminin menzili ve delip geçme konsepti açısından kritik bir spesifikasyondur. Merminin şekli, delinme enerjisinin miktarını etkilemektedir. Bu çalışmada Solidworks akış simülasyon programı kullanılarak, farklı uç şekillerindeki mermiler için hız dağılımı ve türbülans enerjisi araştırılmıştır. Bu çalışmada üç farklı mermi uç şekli incelenmiştir. (Keskin, Yarı yuvarlatılmış, Yuvarlatılmış). Başlangıç hızı tüm durumlar için 500 m/s olarak kabul edilmiştir. Delip geçmenin daha kolay hale geldiği keskin uçlu mermilerin hızdan daha az etkilendiği tespit edilmiştir. Bu çalışmanın sonucunda farklı uç geometrilerine sahip mermiler üzerindeki hız ve basınç dağılımı elde edilmiştir. Mermi ucundaki en fazla hız düşüşü yuvarlatılmış mermi için %57,5 olarak bulunmuştur. Sonuçlar incelendiğinde, hız kaybının keskin tipli mermilerde ve yaklaşık %22,2 olarak bulunduğu açıkça görülmektedir.

**Anahtar Kelimeler:** Hız dağılımı, Türbülans enerjisi, Mermi, Akış simülasyonu, Uç geometrisi

---

\*Sorumlu yazar (Corresponding Author): Mehmet Hanifi DOĞRU, [mhdogru@gantep.edu.tr](mailto:mhdogru@gantep.edu.tr)

## 1. INTRODUCTION

In this section, literature is investigated about analysis with Solidworks Flow Simulation and velocity of the projectile. The projectile shape is a very critical specification in terms of the penetration and range of the bullet. So, in this study, three different projectile tip shapes are analyzed. The literature survey is performed according to this aim. Investigated studies are given below.

The effect of varying the angle of attack on the airfoil and flat shape louvers were investigated by Noh et al. [1]. Airfoil louvers were based on the symmetrical 4 digit NACA airfoil shape and it had 10 mm maximum thickness. CFD analysis was administered by using the built-in Solidworks Flow Simulation to visualize the air flow behavior across the louvers at the angles of attack of 25°, 35°, and 45°. The results revealed that the pressure drop is more prevalent in flat louvers as compared to airfoil louvers.

Arsena et al. [2] investigated how the wind gust affects variation drag resistance to advancing caused by the pantograph and how they affect the supply of electricity required for vehicle movement. EP3 pantograph was modeled geometrically. Solidworks Flow Simulation was used to analyze the effects caused by gusts of wind. Point values for angles were considered in the range of [0°, 180°] and speeds from 0 m/s to 30 m/s.

Experimental validation and numerical simulation were applied to study the turbulent flow around a small incurved Savonius wind rotor by Driss et al. [3]. Solidworks Flow Simulation was utilized to present the local characteristics in different transverse and longitudinal planes. Navier-Stokes equations were used for the numerical models and standard k-ε turbulence model was used. These equations were solved by a finite volume discretization method. Experimental results were manipulated on an open wind tunnel equipped with a small incurved Savonius wind rotor to validate the numerical method.

An acting coordinate method for a multi-domain technique was introduced by Jiang et al. [4] to simulate unsteady flows with moving boundary. The suggested method was used for the flow within the ballistic range. At the end of the study, an interaction between blast wave and shock wave were numerically captured with the prediction of the flying speed of the projectile.

Penetration of a high-speed projectile (>1000 m/s) was investigated in term of the perforation a vessel filled with toxic liquid by Lecysyn et al. [5]. The decay of projectile velocity and projectile-target interactions were examined with the initial conditions of the target.

A projectile, which is supersonic spinning, is affected by boundary layer separation in during the flight time concept was investigated by Rausch et al. [6] and Srivastava [7]. Flight stability of spinning penetrator was examined in terms of the flow separation of the supersonic boundary layer. A standard 155 mm bullet was used for this analysis. The micro-vanes were affixed at the projectile shoulder to investigate the separation control on the aerodynamic characteristics of the projectile. Aerodynamic data and characteristics of the boundary layer structures were discussed and compared by Ma et al. [8].

Induced shock flow concept was investigated using supersonic projectile moving in tubes by Jiang et al. [9]. Euler equations were applied to solve the problem with moving boundary conditions. Numerical work on shock wave flows generated by supersonic projectiles discharging from shock tubes into the ambient air was reported. The interaction of the bow shock wave with the precursor shock wave was emphasized.

An artificial neural network based diagnostic methodology is developed for gas turbine path analysis by Capata [10].

At the end of the literature survey, it is seen that projectile tip geometry is a critical specification in terms of the velocity distribution, pressure distribution and turbulent energy. But when the literature is researched, it is determined that there

is less study about velocity distribution and turbulence energy in the literature. So, this study is concentrated on the investigation of velocity distribution and turbulent energy for the different tip shaped projectile.

## 2. METHODOLOGY

In this study, velocity distribution and turbulence energy of projectile are investigated according to tip geometry of bullet. Three different nose shapes are used to perform the study (sharpen, semi-rounded, and rounded shape). 50 caliber real projectile geometry is used. Initial velocity is accepted as 500 m/s. Solidworks Flow Simulation tool is utilized to execute this work. Dimensions of flow domain are set as +x=12 cm, -x=9 cm, +y=5 cm, -y= 5cm, +z=5 cm and -z=5 cm. External flow is selected to perform the analysis. At the end of the study, velocity distribution, turbulent energy, pressure and mach number are obtained for each case.

Solidworks Flow Simulation is able to consider both laminar and turbulent flows. When the Reynolds number exceeds a certain critical value the flow transitions smoothly to turbulent. To predict turbulent flows, the Favre-averaged Navier-Stokes equations are used, where time-averaged effects of the flow turbulence on the flow parameters are considered, whereas the large-scale, time-dependent phenomena are taken into account directly.

The modified  $k-\varepsilon$  turbulence model with damping functions proposed by Lam and Bremhorst [11] describes laminar, turbulent, and transitional flows of homogeneous fluids consisting of the following turbulence conservation laws as given in equation 1-6.

$$\frac{\partial \rho k}{\partial t} + \frac{\partial \rho k u_i}{\partial x_i} = \frac{\partial}{\partial x_i} \left( \left( \mu + \frac{\mu_t}{\sigma_k} \right) \frac{\partial k}{\partial x_i} \right) + \tau_{ij}^R \frac{\partial u_i}{\partial x_j} - \rho \varepsilon + \mu_t P_B \quad (1)$$

$$\frac{\partial \rho \varepsilon}{\partial t} + \frac{\partial \rho \varepsilon u_i}{\partial x_i} = \frac{\partial}{\partial x_i} \left( \left( \mu + \frac{\mu_t}{\sigma_\varepsilon} \right) \frac{\partial \varepsilon}{\partial x_i} \right) + C_{\varepsilon 1} \frac{\varepsilon}{k} \left( \tau_{ij}^R \frac{\partial u_i}{\partial x_j} + C_B \mu_t P_B \right) - f_2 C_{\varepsilon 2} \quad (2)$$

$$\tau_{ij} = S_{ij} \quad (3)$$

$$\tau_{ij}^R = \mu_t S_{ij} - \frac{2}{3} \rho k \delta_{ij} \quad (4)$$

$$S_{ij} = \frac{\partial u_i}{\partial x_j} + \frac{\partial u_j}{\partial x_i} - \frac{2}{3} \delta_{ij} \frac{\partial u_k}{\partial x_k} \quad (5)$$

$$P_B = - \frac{g_i}{\sigma_B \rho} \frac{\partial p}{\partial x_i} \quad (6)$$

The unstructured mesh method is selected for meshing operation. Mesh number is obtained as 120000 elements according to unstructured mesh method. Mesh validation is performed to obtain realistic results.

### 2.1. Validation of Mesh Number Accuracy

Mesh number is controlled to validate the accuracy of meshing. Mesh indecency is also investigated on the 60000, 120000 and 240000 number of mesh for various downstream of the projectile.

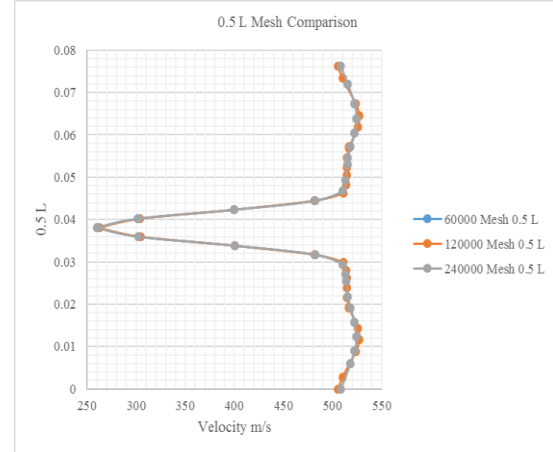


Figure 1. Mesh comparison for 0.5 L

When the Figure 1, Figure 2 and Figure 3 are investigated, it is seen that clearly curves on the figures, which are 60000, 120000 and 240000 mesh number curves, are nearly overlapped. So, It is seen that this study is performed as mesh independence. This mesh independence is shown in Figure 1 for 0.5 L, Figure 2 for L and Figure 3 for 1.5 L.

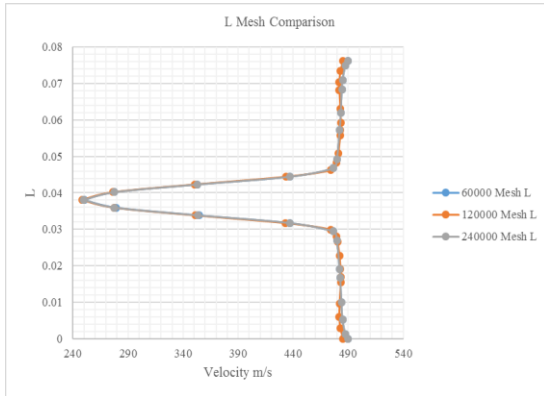


Figure 2. Mesh comparison for L

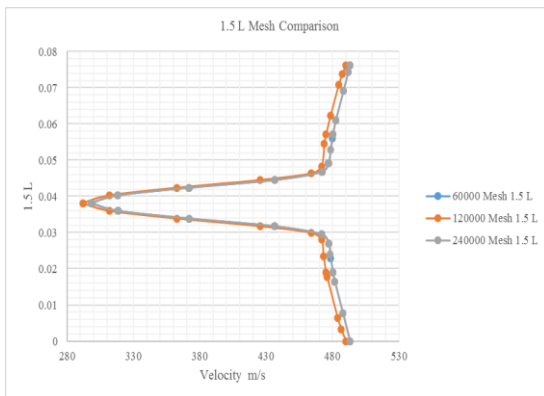


Figure 3. Mesh comparison for 1.5 L

2.1. Case 1

Sharpen type projectile is investigated in the case one as shown in Figure 4. The diameter of the bottom is 13.2 mm, tip round is 1 mm, and length is 61 mm for the sharpen type projectile. At the end of the analysis, pressure is obtained as maximum 144.383 kPa on the tip of the penetrator as shown Figure 4.

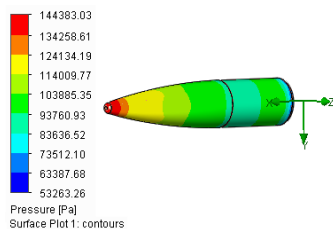


Figure 4. Pressure distribution of sharpen projectile

Velocity distribution is obtained as maximum 490.95 m/s as shown Figure 5. When Figure 2 is investigated, it is clearly seen that velocity value is zero behind the bullet due to the geometry of projectile has edged. The velocity of projectile decreases because of the small flat plane form of the projectile. The velocity value at the tip of the bullet is decreased approximately 22.2%.

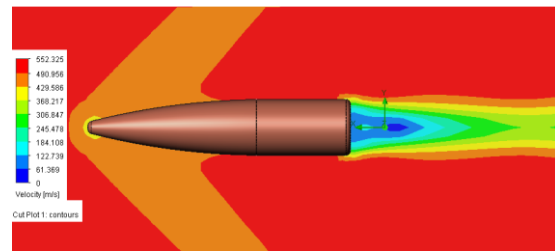


Figure 5. Velocity distribution of sharpen projectile

The amount of energy per unit mass, which is called as turbulent energy, is obtained maximum 5846 J/kg for the sharpen type projectile as shown in Figure 6.

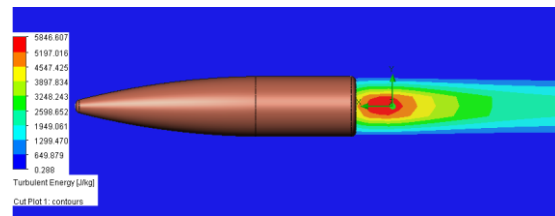


Figure 6. Turbulent energy of sharpen projectile

Mach number is found as maximum 1.68 as shown in Figure 7. Mach number is found as 1.31 at the tip of the projectile. At the tip of the projectile, the flow is found as supersonic due to mach number is between 1.2 and 5 values.

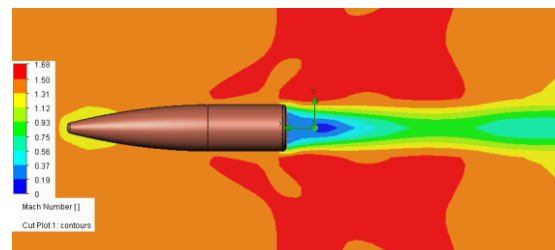
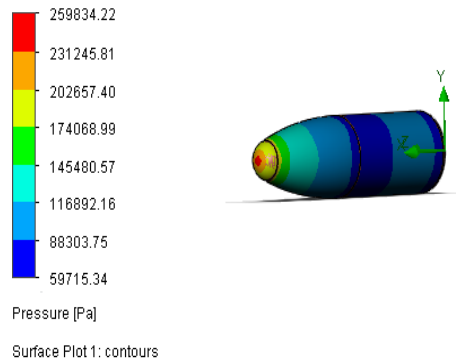


Figure 7. Mach number of sharpen projectile

**2.2. Case 2**

Semi-rounded type projectile is investigated in the case two as shown in Figure 8. At the end of the analysis, pressure is obtained as maximum 259.834 kPa on the tip of the penetrator as shown Figure 8. Diameter of the bottom is 13.2 mm, tip round is 3.3 mm, and length is 42 mm for the semi-rounded type projectile.



**Figure 8.** Pressure distribution of semi-rounded projectile

Velocity distribution is obtained as maximum 467.07 m/s as shown Figure 6. When Figure 9 is investigated, it is seen that velocity value is smaller than case 1 at the stagnation point due to rounded area increase on the semi-rounded type of projectile. Velocity value at the tip of the bullet is decreased nearly 45.6%.

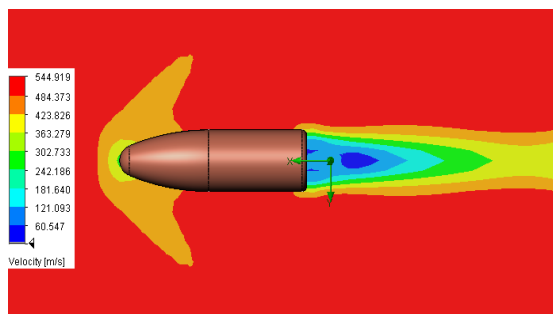


**Figure 9.** Velocity distribution of semi-rounded projectile

Turbulent energy is obtained maximum 6400 J/kg for the semi-rounded type projectile as shown in Figure 10.

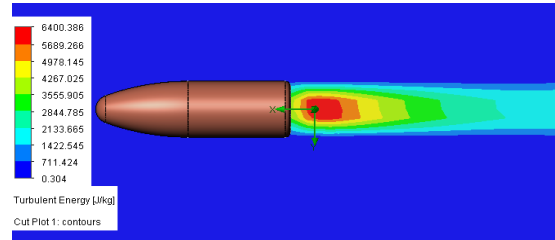


**Figure 10.** Turbulent energy of semi-rounded projectile

Mach number is found as maximum 1.65 as shown in Figure 11. Mach number is found as 0.92 at the tip of the projectile. At the tip of the projectile, the flow is found as transonic due to mach number is between 0.8 and 1.2 values.

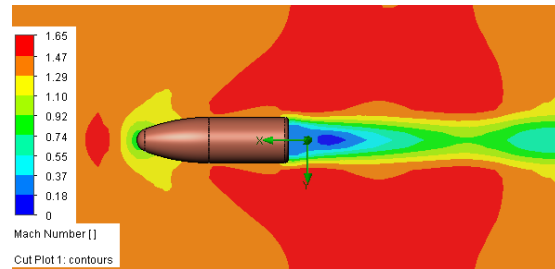


**Figure 11.** Mach number of semi-rounded projectile

**2.3. Case 3**

Rounded type projectile is investigated in the case three as shown in Figure 12. At the end of the analysis, pressure is obtained as maximum 302.185 kPa on the tip of the penetrator as shown Figure 12. The diameter of the bottom is 13.2 mm, tip round is 5.33 mm, and length is 33 mm for the rounded type projectile.

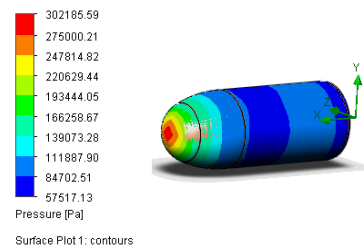


**Figure 12.** Pressure distribution of rounded projectile

Velocity distribution is obtained as maximum 487.01 m/s as shown Figure 13. When Figure 13 is investigated, it is seen that clearly velocity value of rounded type projectile is the smallest in all cases. Velocity value at the tip of the bullet is decreased nearly 57.5%. Separation point has also approached the center of the penetrator.

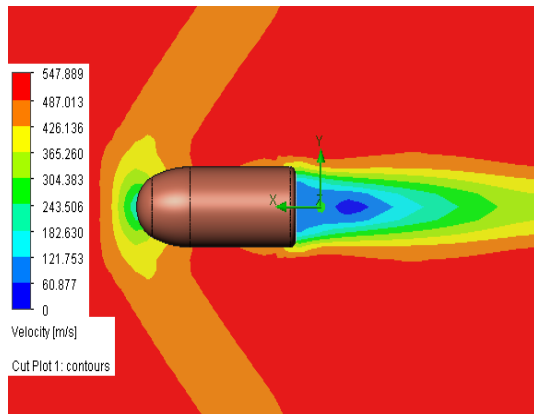


**Figure 13.** Velocity distribution of rounded projectile

Turbulent energy is obtained maximum 6670 J/kg for the semi-rounded type projectile as shown in Figure 14.

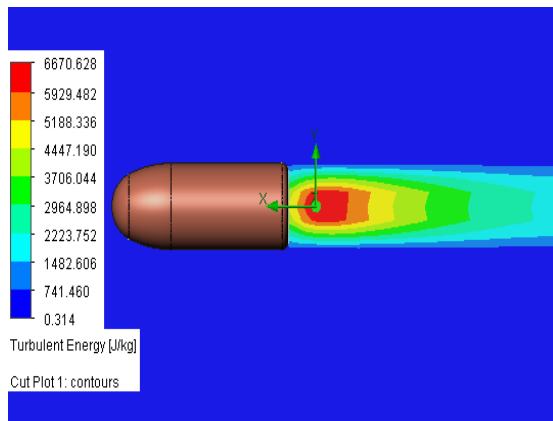


**Figure 14.** Turbulent energy of rounded projectile

Mach number is found as maximum 1.67 as shown in Figure 15. Mach number is found as 0.74 at the tip of the projectile. The maximum decrease of mach number is obtained on the rounded type projectile due to the tip of the projectile is curved

fully. At the tip of the projectile, the flow is found as sonic due to mach number is smaller than 0.8 value.

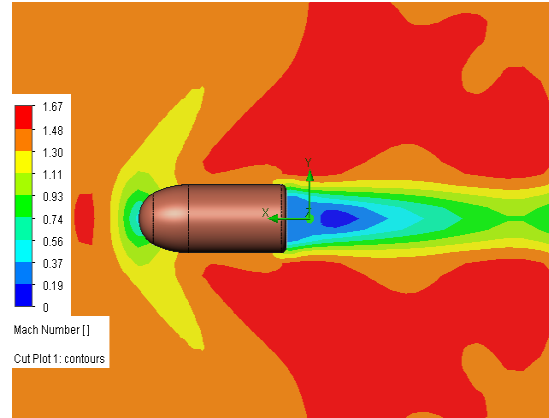


**Figure 15.** Mach number of rounded projectile

### 3. RESULTS AND DISCUSSIONS

In order to better comparison of different shape projectile, it is given dimensionless velocity distribution along to cross-sectional direction (x-axis) at the various location downstream of the projectile (y-axis) as shown Figure 16, Figure 17 and Figure 18.

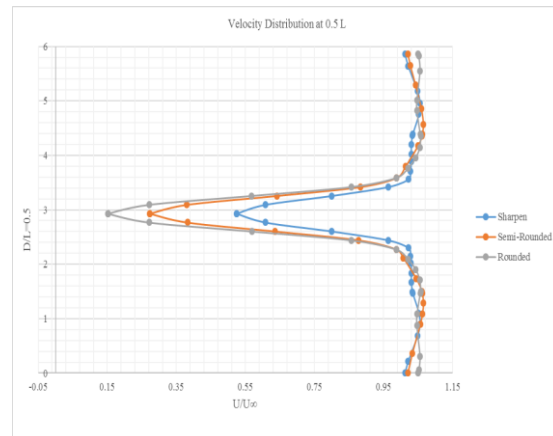


**Figure 16.** Velocity distribution at 0.5 L

There is no significant effect of tip shape of the projectile on the backtrace width. However, the tip shape of the projectile is influential at different cross-sections in the backtrace.

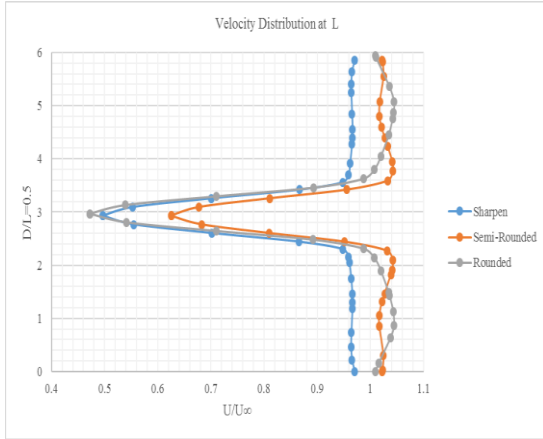


Figure 17. Velocity distribution at L

The lowest velocity profile is obtained for the rounded type of projectile at  $D/L=0.5$  on the backtrace. The velocity values behind the rounded projectile are much higher in terms of values in the x-axis than in other projectiles.

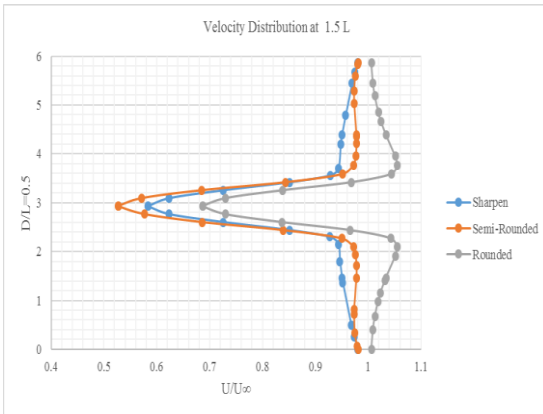


Figure 18. Velocity distribution at 1.5 L

There was no significant difference between the values of  $D/L = 0.5, 1$  and  $1.5$  measured in the distribution of velocity profiles formed behind the sharpen type of projectile.

In this study, different tip shapes of projectile are examined in terms of the velocity distribution and turbulent energy. Three different nose shapes of the projectile are investigated. Velocity loss is given in Table 1 according to the projectile geometry.

Table 1. Numerical results of the study

Projectile Type	Pressure (kpa)	Tip Velocity (m/s)	Mach Number	Velocity Loss (%)
Sharpen	144.38	389.00	1.31	22.2
Semi-rounded	259.38	267.50	0.92	46.5
Rounded	302.19	212.50	0.74	57.5

- The decrease of velocity value at the tip of the bullet is obtained nearly 22.2% on the sharpen type projectile.
- The decrease of velocity value at the tip of the penetrator is found nearly 45.6% on the semi-rounded type projectile.
- The decrease of velocity value at the tip of the projectile is found nearly 57.5% on the rounded type projectile.

Velocity is less affected on the sharpen type projectile, because of the sharpen tip geometry. Therefore, perforation occurs also easily with sharpen tip projectile. It is possible to understand sharpen type projectile has a long flying range. Because the decrease of the velocity is less on sharpen type projectile.

#### 4. CONCLUSIONS

At the end of the study, velocity and pressure distribution on the penetrator, which has different tip geometry, is obtained. When the results are investigated, it is seen that clearly sharpen type projectile is less affected in terms of the velocity loss according to others due to the small flat area on the tip of the projectile. When the cross-sectional area, which is tip area of the projectile, is increased it is seen that pressure increase on the tip of penetrator because of the bigger area. At the end of the study, it is obtained that if projectile has sharpen tip, it has less pressure and less turbulent energy behind the projectile. When the tip area of the projectile is also increased, mach number is also decreased on the tip of the projectile. There is less study on the aerodynamic performance of projectile in the literature. Therefore, this study

will be an important reference for the future studies on the projectile aerodynamics.

## **5. REFERENCES**

1. Noh M.H.M., Rashid H., Hamid A.H.A., Iskandar M.F., 2012. Comparison of Numerical Investigation on Airfoil and Flat Louvers on the Air Duct Intake, *Procedia Engineering*, 41:1761-1768.
2. Arsene S., Sebesan I., Popa G., 2015. The Influence of Wind on the Pantograph Placed on The Railway Vehicles Bodywork, *Procedia-Social and Behavioral Sciences*, 186: 1087-1094.
3. Driss Z., Mlayeh O., Driss D., Maaloul M., Abid M.S., 2014. Numerical Simulation and Experimental Validation of the Turbulent Flow Around a Small Incurved Savonius Wind Rotor, *Energy*, 74:506-517.
4. Jiang Z., Takayama K., Chen Y., 1995. Dispersion Conditions for Non-Oscillatory Shock Capturing Schemes and Its Applications, *Comput. Fluid Dyn., J*, 2:137-150.
5. Lecysyn N., Dandrieux A., Heymes F., Slangen P., Munier L., Lapebie E., Gallic C.L., Dusserre G., 2008. Preliminary Study of Ballistic Impact on an Industrial Tank: Projectile Velocity Decay, *Journal of Loss Prevention in the Process Industries*, 21: 627-634.
6. Rausch J., Roberts B., 1975. Reaction Control System Aerodynamic Interaction Effects on Space Shuttle Orbiter, *Journal of Spacecraft and Rockets*, 12:660-666.
7. Srivastava B., 1998. Aerodynamic Performance of Supersonic Missile Body-and Wing Tip-Mounted Lateral Jets, *Journal of Spacecraft and Rockets*, 35: 278-286.
8. Ma J., Chen Z-h., Huang Z-g., Gao J-g., Zhao Q., 2016. Investigation on the Flow Control of Micro-Vanes on a Supersonic Spinning Projectile, *Defence Technology*, 12:227-233.
9. Jiang, Z., Huang, Y., Takayama, K., 2004. Shocked Flows Induced by Supersonic Projectiles Moving in Tubes, *Computers & fluids*, 33:953-966.
10. Capata R., 2016. An Artificial Neural Network-Based Diagnostic Methodology for Gas Turbine Path Analysis-Part II: Case Study, *Energy, Ecology and Environment* 1:351-359.
11. Lam, C.K.G., Bremhorst, K.A., 1981. Modified Form of Model for Predicting Wall Turbulence, *ASME Journal of Fluids Engineering*, 103:456-460.